Easily fabricated, robust fiber-optic probe for weak fluorescence detection: modeling and initial experimental evaluation

Jianjun Ma,[1,*] Yasser Chiniforooshan,[1] Wenhui Hao,[2] Wojtek J. Bock,[1] and Zhi Yuan Wang[2]

[1] *Centre de recherche en photonique, Département d'informatique et d'ingénierie, Université du Québec en Outaouais, P. O. Box 1250, Hull Station, Gatineau, Québec J8X 3X7, Canada*
[2]*Department of Chemistry, Carleton University, 1125 Colonel By Drive, Ottawa, Ontario, K1S 5B6, Canada*
[*]*ma.jianjun@uqo.ca*

Abstract: Detection of fluorescence from a low quantum yield fluorophore is challenging for a fiber-optic probe, especially when an inexpensive and robust construction is desired. We propose a conceptually straightforward theoretical model to optimize the factors affecting the fluorescence-capture capability of a bifurcated/coaxial fiber-optic probe. Experimentally we verify that such a probe, if optimized, can detect the fluorescence of a polymer fluorophore with a low quantum yield of 0.0065.

OCIS codes: (060.2370) Fiber Optics Sensors; (300.6280) Spectroscopy, fluorescence and luminescence; (060.2270) Fiber characterization.

References and links

1. B. A. Flusberg, E. D. Cocker, W. Piyawattanametha, J. C. Jung, E. L. M. Cheung, and M. J. Schnitzer, "Fiber-optic fluorescence imaging," Nat. Methods **2**(12), 941–950 (2005).
2. M. G. Shim, B. C. Wilson, E. Marple, and M. Wach, "Study of fiber-optic probes for in vivo medical Raman spectroscopy," Appl. Spectrosc. **53**(6), 619–627 (1999).
3. L. Wen-xu and C. Jian, "Continuous monitoring of adriamycin in vivo using fiber optic-based fluorescence chemical sensor," Anal. Chem. **75**(6), 1458–1462 (2003).
4. T. F. Coony, H. T. Skinner, and S. M. Angel, "Comparative study of some fiber-optic remote Raman probe designs. Part I: model for liquids and transparent solids," Appl. Spectrosc. **50**(7), 836–848 (1996).
5. U. Bunting, F. Lewitzka, and P. Karlitschek, "Mathematical model of a laser-induced fluorescence fiber-optic sensor head for trace detection of pollutants in soil," Appl. Spectrosc. **53**(1), 49–56 (1999).
6. K. R. Rogers and E. J. Poziomek, "Fiber optic sensors for environmental monitoring," Chemosphere **33**(6), 1151–1174 (1996).
7. J. Ma and W. Bock, "Modeling of photonic crystal fiber with air holes sealed at the fiber end and its application to fluorescent light collection efficiency enhancement," Opt. Express **13**(7), 2385–2393 (2005).
8. X. B. Zhang, C. C. Guo, Z. Z. Li, G. L. Shen, and R. Q. Yu, "An optical fiber chemical sensor for mercury ions based on a porphyrin dimer," Anal. Chem. **74**(4), 821–825 (2002).

1. Introduction

A fiber-optic probe wins over other means for chemical species analysis due to its well-known advantages: it is lightweight, flexible, non-toxic, low-loss, cost-effective and has a remote-monitoring capability. These features make it possible to construct an elegant hand-held probe for on-site chemical species assay in various environments [1–8].

A bifurcated fiber probe [3–8] or its improved version, a coaxial fiber probe [3, 4], is often adopted for chemical species assay, whose configuration is shown in Figs. 1(a) and 1(b), respectively. Either probe architectures could be easily constructed without sophisticated facilities. Its tiny probing end packs, for example, two or seven 430 μm fibers and the protecting sleeve into a cylinder approximately 2 mm in diameter. This small dimension makes bifurcated/coaxial fiber-optic probes widely used for chemical and biological species investigations and for *in vitro/vivo* detection [1–8]. However, the discussions in the relevant research papers seldom evaluate how well the flat-tipped probe detects the weak signal from a low quantum-yield fluorophore. Instead, a popular solution to cope with the weak fluorescent

#162195 - $15.00 USD Received 26 Jan 2012; accepted 2 Feb 2012; published 10 Feb 2012

power is to use a fiber-optic probe with a better ability to capture light, such as one with a beveled probing tip. However, in comparison to the flat-tipped probe, the bevel-tipped end is hard to fabricate and offers poor protection of the sensing area. Given these issues, we investigate the use of the flat-tipped coaxial fiber-optic probe to detect the fluorescent signal of the low quantum-yield fluorophore under the simplest procedures and at the lowest possible cost. The fluorophore is a low band-gap polymer, represented here by P1, which contains a D-π-A system and has a low quantum yield ($Q = 0.0065$).

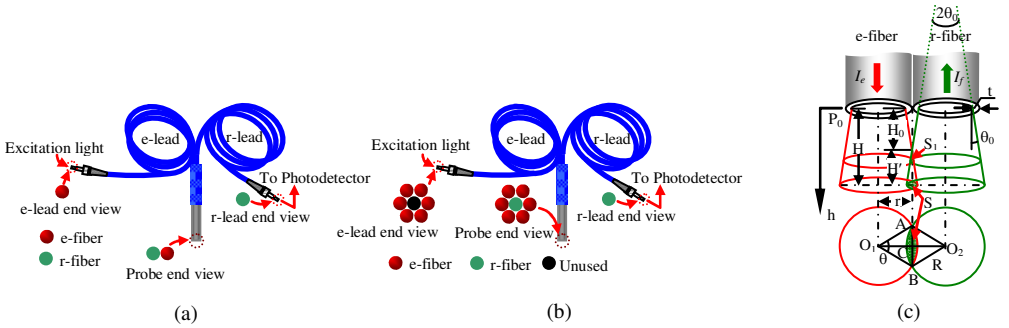

Fig. 1. Bifurcated and co-axial fiber-optic probes. (a) Typical bifurcated fiber-optic probe. (b) Coaxial fiber-optic probe for enhanced light collection. (c) The bifurcated fiber-probe with parameters for theoretical analysis. Only one overlapping volume is available to capture fluorescent power. S_1 and S (shaded) are two cross sections of this volume. In contrast to (c), six identical active volumes (not drawn) and thus six active areas are available for a coaxial fiber-optic probe, leading to a six-fold increase of the overall captured fluorescent power.

2. Improving the bifurcated/coaxial fiber-optic probe for low quantum-yield fluorescence detection

Detection of weak fluorescence requires an optimized coaxial fiber-probe with enhanced ability to capture light. To date, this subject has been investigated by a number of papers, with references 4 and 5 being perhaps the most rigorous and comprehensive but very complicated. In this paper, we propose a straightforward and intuitive approach to calculating the fluorescent-power capture ability of a flat-tipped bifurcated/coaxial fiber probe as shown in Fig. 1. Figure 1(c) gives detailed information on the two architectures required for the theoretical investigation. The excitation light and the captured signal light are limited respectively by the excitation cone (e-cone) and the receiving cone (r-cone) represented by $2\theta_0$. In the most common construction, which has two identical fibers, the angles of these two cones that open to the sample are equal and determined by their numerical aperture $NA = n\sin\theta_0$, where n is the refractive index (RI) of the sample. The e-cone starts to overlap with the r-cone at the distance H_0 from the probe tip. It is obvious that the captured fluorescent light from the sample can only arises from this overlapping or active volume. The shape of this active volume could be understood from the overlapping or active areas of S_1 and S , which are formed by two cross sections of the two cones. The excitation power density P_{e_d} varies from H_0 to H, or obeys:

$$P_{e\_d} = P_{e\_d}(h) \neq const. \tag{1}$$

Thus the fluorescent power I_f' should be expressed by:

$$I_f' \propto \int_{H_0}^{H} P_{e\_d}(h) \cdot S(h) \cdot dh \tag{2}$$

#162195 - $15.00 USD
Received 26 Jan 2012; accepted 2 Feb 2012; published 10 Feb 2012

Obviously, Eq. (2) has to include the factors representing the characteristics of the fluorophore. For a diluted solution, I'_f is related to the excitation power intensity I_e, molar absorptivity ε, quantum yield Q, the concentration c and the path length l by:

$$I'_f = k \cdot Q \cdot I_e \cdot \varepsilon \cdot c \cdot l \tag{3}$$

where k is a constant coefficient that may be determined by calibration. By applying Eq. (3) to Fig. 1(c), the total fluorescence power captured in the volume $S(h) \cdot dh$ at any depth $h\,(H_0 < h \le H)$ could be written as:

$$dI'_f = k \cdot Q \cdot I_e(h) \cdot \varepsilon \cdot c \cdot dh = k \cdot Q \cdot \left[P_{e\_d}(h) \cdot S(h) \right] \cdot \varepsilon \cdot c \cdot dh \tag{4}$$

where

$$I_e(h) = P_{e\_d}(h) \cdot S(h) \tag{5}$$

Clearly, Eq. (4) is equivalent with Eq. (2) but includes detailed information describing the fluorescence-capable solution.

Equation (5) indicates the overall excitation power incident on the overlapping area $S(h)$ at depth $h\,(H_0 < h \le H)$ while Eq. (4) assumes that within the small thickness dh the value $I_e(h)$ remains unchanged.

To simplify the discussion (a reasonable approach for a diluted solution), we ignore the attenuation of the excitation power when traveling in the solution, and thus:

$$P_{e\_d}(h) \cdot S(h) = P_{e\_d}(0) \cdot S(0) \tag{6}$$

In contrast to the rigorous but complex treatment of the excitation light beam in [4], Eq. (6) assumes a uniform distribution of excitation power across the entire cross section of the light beam, which not only greatly simplifies the derivation, but also makes the concept easier to understand. Any error associated with this approximation is likely due to overestimating the excitation power in the overlapping volume, and could be greatly reduced by including the power penalty factor in the coefficient k in Eq. (4). Critically, since all calculation results given later (Fig. 2) are based on ratio to obtain normalized intensities and thus allow the coefficient k to be cancelled out. From this point of view, the results from such an approximation provide a satisfactory degree of accuracy.

With $S(0) = \pi r^2$ and $S(h) = \pi R^2$, where r and R are the radius of the fiber core and the radius of the cross section of the e-cone or r-cone at the depth $h\,(H_0 < h \le H)$, we can write:

$$P_{e\_d}(h) = P_{e\_d}(0) \cdot \left(\frac{r}{R} \right)^2 \tag{7}$$

Any overlapping area $S(h)$ has the same the geometry as $S = S(H)$ in Fig. 1(c). The following expression is not difficult to find:

$$S(h) = 2 \cdot \left[R^2 \cdot \sec^{-1}\left(\frac{R}{r} \right) - r\sqrt{R^2 - r^2} \right] \tag{8}$$

Replacing the associated terms in Eq. (4) with Eqs. (7) and Eq. (8) yields:

$$dI'_f(h) = 2 \times k \cdot Q \cdot P_{e\_d}(0) \cdot \left(\frac{r}{R} \right)^2 \cdot \left[R^2 \cdot \sec^{-1}\left(\frac{R}{r} \right) - r\sqrt{R^2 - r^2} \right] \cdot \varepsilon \cdot c \cdot dh \tag{9}$$

#162195 - $15.00 USD Received 26 Jan 2012; accepted 2 Feb 2012; published 10 Feb 2012

By assuming $\gamma = 2\times k\cdot Q\cdot \varepsilon \cdot c\cdot P_{e\_d}(0)$ and lossless transmission of dI'_f from depth $h=H$ to $h=0$, the captured fluorescent power at the entrance of the r-fiber $(h=0)$, represented by $I_f(h=0)$, could be straightforwardly written from Eq. (9):

$$I_f(h=0)=\gamma\cdot\int_{H_0}^{H}\left[\left(\frac{r}{R}\right)^2\cdot\left(R^2\cdot\sec^{-1}\left(\frac{R}{r}\right)-r\sqrt{R^2-r^2}\right)\right]\cdot dh \tag{10}$$

We change Eq. (10) to the form:

$$I_f(h=0)=\gamma\cdot r^2\int_{H_0}^{H}\left[\sec^{-1}\left(\frac{R}{r}\right)-\frac{r}{R}\sqrt{1-\left(\frac{r}{R}\right)^2}\right]\cdot dh \tag{11}$$

Figure 1(c) validates the following relations:

$$R=h\cdot tg\theta_0+r,\ h=(R-r)\cdot ctg\theta_0, \tag{12}$$

For $h=H_0=t\cdot ctg\theta_0$, Eq. (12) gives $R_0=r+t$, where t is the cladding thickness.

Equation (11) thus becomes:

$$\begin{aligned} I_f(h=0)&=\gamma\cdot r^2\int_{R_0}^{R}\left[\sec^{-1}\left(\frac{R}{r}\right)-\frac{r}{R}\sqrt{1-\left(\frac{r}{R}\right)^2}\right]\cdot d\left[(R-r)\cdot ctg\theta_0\right]\\ &=\gamma'\cdot\int_{R_0}^{R}\left(\sec^{-1}\left(\frac{R}{r}\right)-\frac{r}{R}\sqrt{1-\left(\frac{r}{R}\right)^2}\right)\cdot dR \end{aligned} \tag{13}$$

where $\gamma'=\gamma\cdot r^2\cdot ctg\theta_0$

Equation (13) is further simplified by assuming $u=\frac{R}{r}$ and $w=\frac{r}{R}$:

$$I_f(h=0)=\gamma'\cdot\left\{r\cdot\int_{\frac{R_0}{r}}^{\frac{R}{r}}\sec^{-1}u\cdot du-r\int_{\frac{r}{R_0}}^{\frac{r}{R}}w\sqrt{1-w^2}\cdot d\frac{1}{w}\right\} \tag{14}$$

Assuming $I_f=I_f(h=0)$ Eq. (14) yields:

$$\begin{aligned} I_f=&\gamma''\cdot\left\{\left[\frac{R}{r}arc\sec\frac{R}{r}-\ln\left(\frac{R}{r}+\sqrt{\left(\frac{R}{r}\right)^2-1}\right)\right]-\left[\frac{R_0}{r}arc\sec\frac{R_0}{r}-\ln\left(\frac{R_0}{r}+\sqrt{\left(\frac{R_0}{r}\right)^2-1}\right)\right]\right\}\\ &+\gamma''\cdot\left\{\left[\sqrt{1-\left(\frac{r}{R}\right)^2}-\ln\frac{1+\sqrt{1-\left(\frac{r}{R}\right)^2}}{\frac{r}{R}}\right]-\left[\sqrt{1-\left(\frac{r}{R_0}\right)^2}-\ln\frac{1+\sqrt{1-\left(\frac{r}{R_0}\right)^2}}{\frac{r}{R_0}}\right]\right\} \end{aligned} \tag{15}$$

where

$$\gamma''=2\times k\cdot Q\cdot\varepsilon\cdot c\cdot P_{e\_d}(0)\cdot r^3\cdot ctg\theta_0 \tag{16}$$

Equation (15) expresses the overall fluorescent power captured by the r-fiber from the overlapping volume between H_0 and H for a lossless liquid solution. For a coaxial fiber-optic

#162195 - $15.00 USD Received 26 Jan 2012; accepted 2 Feb 2012; published 10 Feb 2012

probe, there are six identical overlapping volumes that contribute to the overall captured fluorescent power. In this case, we can write:

$$I_{f\_coaxial} = 6 \cdot I_f \tag{17}$$

The calculation of Eqs. (15) and Eq. (16) generates the results presented in Fig. 2, from which we can draw the following conclusions. First, the core radius r greatly affects I_f via r^3, which is reflected by all curves in Figs. 2(a), 2(b), 2(c), 2(e) and 2(f). Second, from Figs. 2(a) and 2(b), when a greater detecting depth H is considered, which is meaningful for an extremely low or a lossless sample medium, cladding thickness variation affects I_f on a smaller scale. This becomes obvious when a larger core fiber is involved. A core radius as small as 5 μm, as in a single-mode fiber, yields $I_f \to 0$ for any cladding thickness. Third, a larger *NA* could lead to a better capturing capability via $ctg\theta_0$ as described by Fig. 2(c), which also indicates a rapid rise of I_f for a larger core fiber. Fourth, the benefit of a large *NA* also includes a shorter initial depth H_0, as shown in Fig. 2(d). The depth H_0 is proportional to the dead space in front of the probe tip. While this might not be a concern for lossless medium such as we assume in this paper for Eqs. (10) and (15), when a lossy medium fills this space – as in fact occurs to most samples – Eqs. (10) and (15) must include the attenuation coefficients for both excitation and fluorescent power, and $I_f << I_f'$ may result. Fifth, instead of altering the *NA*, using a smaller cladding thickness t is another efficient way to reduce the dead space, as indicated in Fig. 2(d). This is perhaps a more meaningful option since all spectrometers accepting fiber-optic connection are designed for $NA = 0.22$, which is the lowest *NA* found in Figs. 2(c) and 2(d). For this reason, Fig. 2 emphasizes the results for $NA = 0.22$. Sixth, the standard multimode fiber for fiber-optic communication, with its core/cladding diameter of 50 / 125 μm and $NA = 0.22$, is an inexpensive and convenient fiber to use in construction of the bifurcated/coaxial fiber-optic probe. However, the limited capability of this fiber to capture fluorescent power, as evidenced in Fig. 2(e), contrasts with the fluorescence-capture ability of the fiber with core/cladding diameter of 400/430 μm and $NA = 0.22$ used here. Seventh, the high performance of the fiber-optic probe presented in this work is evident in all parts of Fig. 2. For the reasons outlined above, this must be considered the optimal design taking into account all the factors discussed so far.

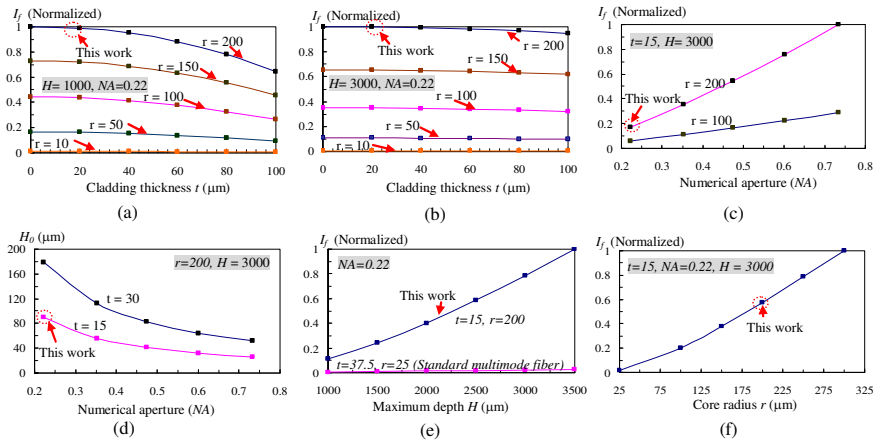

Fig. 2. Some important conclusions from Eq. (15) are illustrated here. The data points or curve labeled as "This work" are associated with the coaxial fiber-optic probe in our experiment. The shaded areas of each figure indicate the parameters fixed for all curves in that figure. (a) Normalized captured power I_f at $h = 0$ vs. cladding thickness when H = 1000 μm. (b) Same as (a) except H = 3000 μm. (c) Impact of *NA* on I_f for two fibers, one with r = 100 μm, the other with r = 200 μm. (d) Impact of *NA* on initial depth H_0 defined in Fig. 1(c), which describes the dead space in front of the fibers. (e) I_f vs the maximum detection depth H for the fiber used in this work and for the standard multimode fiber in fiber-optic communication. (f) Significant impact of fiber core radius r alone on I_f for fixed t, *NA* and H.

#162195 - $15.00 USD Received 26 Jan 2012; accepted 2 Feb 2012; published 10 Feb 2012

3. Experiments and discussions

A P1 solution is prepared by dissolving 2.9 mg P1 in 1 ml of $CHCL_3$ and stirring for one hour and further diluted in 10 ml DMF solvent. After filtering, the P1 solution (3×10^{-4} M) is ready. For the purpose of performance comparison, we also prepared a rhodamine 6G (R6G) water solution (29 μg / ml) as the high quantum-yield ($Q = 0.95$) fluorophore.

The coaxial fiber-optic probe shown in Fig. 1(b), with optimized performance as illustrated in Fig. 2, is used for fluorescence measurement. All fibers are identical, having a core/cladding diameter of 400/430 μm and *NA* of 0.22. The excitation light (633 nm for P1 and 532 nm for R6G) is launched to the e-lead that comprises six e-fibers surrounding one r-fiber in the probing end. The r-fiber constitutes the r-lead and is connected to an Ocean Optics QE65000 spectrometer, which is interrogated by a laptop via USB connection. The Ocean Optics SpectraSuite software package is used to record the fluorescence spectra.

In the first experiment, the fluorescent spectrum is recorded by immersing the fiber probing tip into the R6G solution. Similarly, the second experiment is carried out by immersing the probing end into the P1 solution. The experimental result in Fig. 3(a) shows that the R6G affords a high quality fluorescent spectrum owing to its high quantum yield (Q = 0.95*)* that requires only 3 ms integration time, with complete elimination of the excitation laser trace even without an emission filter. Yet, despite the very low quantum yield (Q = 0.0065) of the P1 solution, which produces a fluorescent power 150 times weaker than R6G, Fig. 3(b) indicates that the optimized coaxial probe is still able to capture the fluorescent spectrum from P1, albeit with an integration time of 5,000 ms. However, this 5,000 ms integration time leads to a strong excitation-power trace in the captured spectrum in Fig. 3(b), an effect stemming from the limitation of the fiber probe itself. Since a fiber-optic-based system affords many well known advantages but at the cost of an enormous power penalty during both excitation and fluorescent light coupling, a high integration time is needed in order for the QE65000 spectrometer to respond to the weak P1 fluorescence.

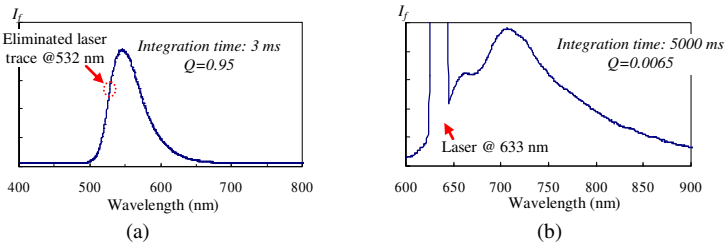

Fig. 3. Fluorescence spectra of R6G and P1 in DMF captured by the optimized coaxial fiber-optic probe. (a) Strong and high quality fluorescence of R6G without an excitation laser trace; (b) Weak fluorescence of P1 with a strong excitation laser trace. Note the significant differences in their integration times and the quantum yields.

4. Conclusions

In conclusion, this paper proposes a straightforward model for calculating and optimizing the ability of a coaxial fiber-optic probe to capture fluorescent light from a lossless liquid. The analytical expression obtained shows how the captured fluorescent power is affected by such important parameters as the molar absorptivity, the sample concentration, the quantum yield, the excitation power intensity, the dimensions of the fiber core and cladding, and the value of *NA*. The fiber parameters for maximum possible fluorescent power capture, presented here in a series of graphs, could be used to optimize the fiber-optic probe by matching the demands of various measurement environments and a particular spectrometer design. Evaluation of the performance of the coaxial fiber-optic probe optimized on the basis of this model shows a satisfactory quality of the fluorescence spectrum captured from a polymer fluorophore with an

#162195 - $15.00 USD Received 26 Jan 2012; accepted 2 Feb 2012; published 10 Feb 2012

extremely low quantum yield of 0.0065. The lowest concentration this probe can cope with is 3×10^{-4} M.

The work presented here paves the way towards using the coaxial fiber probe to detect trace heavy metal by turning on and off fluorescence of this P1 polymer via titration measurement, which will be discussed in our next paper.

Acknowledgments

The authors gratefully acknowledge support for this work from the Natural Sciences and Engineering Research Council of Canada, from the Canada Research Chairs Program and from the Ministère de Développement économique, Innovation et Exportation du Québec.

#162195 - $15.00 USD Received 26 Jan 2012; accepted 2 Feb 2012; published 10 Feb 2012